

Structural Parameters and Dynamical Masses for Globular Clusters in M33 ¹

Søren S. Larsen and Jean P. Brodie

UC Observatories / Lick Observatory, University of California, Santa Cruz, CA 95064, USA

soeren@ucolick.org and brodie@ucolick.org

and

Ata Sarajedini

Department of Astronomy, University of Florida, 211 Bryant Space Science Center, P. O. Box 112055, Gainesville, FL 32611-2055, USA

ata@polaris.astro.ufl.edu

and

John P. Huchra

Harvard-Smithsonian Center for Astrophysics, USA

huchra@fang.harvard.edu

ABSTRACT

Using high-dispersion spectra from the HIRES echelle spectrograph on the Keck I telescope, we measure velocity dispersions for 4 globular clusters in M33. Combining the velocity dispersions with integrated photometry and structural parameters derived from King–Michie model fits to WFPC2 images, we obtain mass-to-light ratios for the clusters. The mean value is $M/L_V = 1.53 \pm 0.18$, very similar to the M/L_V of Milky Way and M31 globular clusters. The M33 clusters also fit very well onto the fundamental plane and binding energy – luminosity relations derived for Milky Way GCs. Dynamically and structurally, the four M33 clusters studied here appear virtually identical to Milky Way and M31 GCs.

Subject headings: galaxies: star clusters — galaxies: individual (M33)

¹Based on data obtained at the W.M. Keck Observatory, which is operated as a scientific partnership among the California Institute of Technology, the University of California and the National Aeronautics and Space Administration.

1. Introduction

In the Local Group, by far the best studied globular cluster (GC) systems are those of the Milky Way and M31. Significant amounts of data have been gathered for globular clusters in these galaxies, with extensive compilations in Harris (1996) (Milky Way, 147 clusters) and Barmby et al. (2000) (M31, 435 clusters). Both of these large spirals are known to contain two distinct GC subpopulations: a metal-poor halo population and a more metal-rich population, associated with the bulge or thick disk (Kinman 1959; Zinn 1985; Minniti 1995; Jablonka et al. 1998; Perrett et al. 2002). The presence of two GC subpopulations presumably indicates different formation processes, and may hold clues to the formation and early evolution of the host galaxies. A particularly controversial issue is whether or not age differences exist between globular clusters of different metallicities. In M31, Barmby & Huchra (2000) found evidence for age differences of 4–8 Gyrs between the metal-rich and metal-poor clusters and Sarajedini, Chaboyer, & Demarque (1997) concluded that a similar age spread exists among GCs in the Milky Way. Other recent studies have proven less conclusive, but age differences of a few Gyrs cannot be ruled out (Stetson, Vandenberg, & Bolte 1996; Buonanno et al. 1998; Rosenberg et al. 1999).

The GC system of the third spiral galaxy in the Local Group, M33, is more sparse and consequently more difficult to identify and study. Early work on the star clusters in this galaxy was done by Hiltner (1960) and Kron & Mayall (1960), who noted that some of them had unusually blue colors. Photometry for about 130 cluster candidates was given by Christian & Schommer (1982, 1988), who tentatively identified 27 old GC candidates in M33. They also noted that M33 appears to contain a number of “blue populous” clusters similar to those in the Large Magellanic Cloud (Hodge 1961), but without the pronounced age gap that exists between ~ 3 Gyrs and 12–15 Gyrs in the LMC (Girardi et al. 1995). The old GCs exhibit halo-like kinematics, while the younger clusters follow the rotation of the disk (Schommer et al. 1991). Color-magnitude diagrams for 10 halo GCs in M33, obtained with WFPC2 on board HST, were presented by Sarajedini et al. (1998), who noted that most of the clusters showed no blue horizontal branches in spite of having low metallicities. They suggested that this might be due to a second-parameter effect, indicating that many of the “old” M33 clusters may be several Gyrs younger than their Galactic counterparts. Additional clusters have been identified on WFPC2 images by Chandar, Bianchi, & Ford (2001), and again Chandar et al. (2002) suggested a larger age spread among the halo GCs compared to the Milky Way.

It is important to establish how much the old globular clusters in different galaxies have in common. A larger age spread among halo GCs in M33, for example, might indicate that this galaxy assembled over a longer period of time, while the structure of individual clusters may provide information about the gas clouds out of which they formed (Murray & Lin 1992; Elmegreen & Efremov 1997). In the Milky Way, a number of fundamental correlations are known to exist between parameters such as surface brightness, core radius and velocity dispersion of globular clusters (Kormendy 1985; Djorgovski 1995). McLaughlin (2000) found that all Milky Way GCs are consistent with a constant V -band core mass-to-light ratio (within the error margins) of 1.45

$M_{\odot} L_{\odot}^{-1}$. He also found a tight relation between the binding energy of individual clusters and the total luminosity, with a weak decrease in binding energy as a function of Galactocentric distance. The dependence on Galactocentric distance may hold information about pressure gradients in the early Galactic halo.

Detailed information about the structure of extragalactic GCs, even within the Local Group, is more limited for obvious reasons. At the distance of M31 and M33, a typical ground-based resolution of $\sim 1''$ corresponds to a linear scale of about 4 pc, roughly similar to the typical half-light radii of globular clusters. Thus, information about the detailed structure of individual clusters is not easily obtained. However, with the HST the situation is greatly improved, with one pixel on the Planetary Camera (PC) corresponding to about 0.2 pc. This is of great importance not only for studies aiming at a morphological characterization of the clusters, but also for dynamical studies in which velocity dispersions must be tied to knowledge about the cluster structure in order to provide accurate mass-to-light ratios. So far, the mass-to-light ratios and other properties of globular clusters in M31 appear to be identical to those observed in Milky Way GCs (Djorgovski et al. 1997; Dubath & Grillmair 1997; Barmby, Holland, & Huchra 2002). Similarity in the M/L ratios (modulo metallicity effects) is, of course, to be expected if the clusters have similar ages, unless there are variations in the stellar mass function. No information about dynamical masses has yet been published for M33 GCs, but could potentially be used as a tool to independently check whether age differences exist.

In this paper we study 4 globular clusters in M33, selected from the sample of Sarajedini et al. (1998). The clusters were originally selected based on their halo-like kinematics and red colors ($B-V > 0.6$), and should be as close an analogy to the halo clusters in the Milky Way as possible. We use new high-dispersion spectroscopy from the HIRES spectrograph on the Keck I telescope to measure velocity dispersions for the individual clusters, and combine these with structural information from the same HST images used by Sarajedini et al. (1998) to derive mass-to-light ratios and compare with data for Milky Way globular clusters. Throughout the paper we will adopt a distance modulus of 24.84 and the reddenings for each cluster determined by Sarajedini et al. (2000).

2. Data

Observations of the four clusters (R12, H38, M9 and U49) were carried out on Oct 24 and 25, 1998 with the HIRES spectrograph (Vogt et al. 1994) on the Keck I telescope. A slit width of $0''.725$ was used, providing a spectral resolution of $\lambda/\Delta\lambda \approx 54000$. The wavelength range was 3730–6170 Å, distributed over 38 echelle orders, although a useful S/N was achieved only for $\lambda \gtrsim 4000$ Å. For each cluster, 7–8 individual exposures of 1800 s each were obtained. In addition, the star HD 1918 (G9 III) was observed as a template star for the velocity dispersion measurements.

Extraction of the spectra from the CCD images was done with the highly automated MAKEE

package, written by T. Barlow and specifically tailored for reduction of HIRES data. MAKEE automatically performs bias and flatfield corrections, cleans the images of cosmic-ray (CR) hits and then locates and extracts each echelle order from the CCD images. Wavelength calibration was done using spectra of ThAr calibration lamps mounted within HIRES, with zero-point corrections based on sky lines. The individual 1d spectra of each cluster were co-added using a sigma-clipping algorithm to eliminate any residual CR events, producing a S/N for the co-added spectra of 15–25 per resolution element.

2.1. Velocity dispersions

A variety of techniques have been developed to measure velocity dispersions from integrated spectra in cases like ours where the expected dispersions (5–10 km/s) are comparable to the instrumental resolution. The most direct method is to simply convolve the template star spectrum with Gaussian profiles corresponding to different velocity dispersions, and then find the velocity dispersion that minimizes the residuals when the (scaled and smoothed) template star spectrum is subtracted from the cluster spectrum. One appealing aspect of this method is that the quality of the fit and the match between template and object spectra can be readily inspected, but the velocity dispersions are quite sensitive to an accurate determination of the velocity difference between the two objects as well as a good match between the cluster and template spectra. Alternatively, the fitting can be done in the Fourier domain (Illingworth 1976), utilizing the fact that the slope of the power spectrum is strongly sensitive to the spectral resolution. A third method is to cross-correlate the cluster spectrum with the template spectrum and use the width of the cross-correlation peak as an indicator of the velocity dispersion (Tonry & Davis 1979; Ho & Filippenko 1996). Yet another technique was used by Dubath & Grillmair (1997), who convolved the cluster spectrum with a suitably designed mask to obtain a “mean” spectral line whose width is related to the velocity dispersion.

The method of directly fitting a smoothed template spectrum to the cluster spectrum is illustrated in Figure 1, where we compare two echelle orders of the spectrum of cluster H38 with the template star. Each panel shows the cluster spectrum, the template star spectrum, the best-fitting smoothed template star spectrum and the residuals. Even though the smoothing results in a much better fit than the raw template spectrum, indicating that the broadening of lines in the cluster spectrum due to velocity dispersion is well resolved, significant residuals are still visible for many of the stronger lines. There are no systematic trends in the residuals (some are positive, others negative), but the template star is evidently not an ideal match to the cluster spectrum.

We also measured velocity dispersions with the cross-correlation method, using the FXCOR task in the RV package in IRAF². This method is less dependent on an exact match between the

²IRAF is distributed by the National Optical Astronomical Observatories, which are operated by the Association

cluster and template spectra, because a poorer match will tend to change the amplitude rather than the width of the cross-correlation peak. In Fig. 2 we show the cross-correlation functions (CCFs) for cluster H38 (order 28) vs. the template star (solid line), as well as the CCFs for the template star spectrum broadened with three different Gaussians (0, 6 km/s, 12 km/s) vs. the template star spectrum itself (dashed lines). The best fit is obtained for a velocity dispersion around 6 km/s. As a useful “byproduct”, the cross-correlation technique automatically provides radial velocities for the clusters, which are needed as input for the other methods.

Line-of-sight velocity dispersions (σ_x) are listed in Table 1 for both the direct fitting and cross-correlation techniques. The σ_x values are averaged over all fitted echelle orders, with the number of echelle orders used for the fits listed in column (2). We give both the rms scatter of the σ_x values measured on the individual echelle orders, as well as the formal standard errors on the mean. However, many of the uncertainties, related to choice of template star, fitting technique etc. are systematic rather than random, and simply estimating the uncertainties from the scatter between the various echelle orders may not give a realistic estimate of the true uncertainties. Table 1 also lists the radial velocities of the clusters and measurements from Schommer et al. (1991) and Chandar et al. (2002) for comparison. The dominating uncertainty on our radial velocity measurements is actually the radial velocity of the template star itself, given as $+35.7 \pm 2$ km/s in SIMBAD. For all clusters except H38, our radial velocities agree with those of Chandar et al. (2002) within the errors. The mean difference between our measurements and theirs is 19 ± 13 km/s.

As seen in Table 1, the cross-correlation technique gives systematically lower velocity dispersions than the direct fitting, with differences of 0.4 – 0.9 km/s. We tested the direct fitting method by artificially broadening a template star spectrum, adding noise and applying the fitting algorithm to the resulting spectrum. The dispersions of the Gaussians used for the smoothing were reproduced with an accuracy of better than 0.1 km/s for a S/N similar to that of the cluster spectra. For even lower S/N the accuracy decreased, but no systematic trends were evident. However, we note that one pixel corresponds to a velocity difference of about 2.0 km/s, so the difference between the two methods may well be due to centering and/or binning effects. Direct fitting is more sensitive to such effects than the cross-correlation technique and we may assume that the latter is more accurate. In the following discussion we therefore adopt the velocity dispersions obtained by the cross-correlation method.

2.2. Structural parameters

To obtain structural parameters for the clusters we used images from the Wide Field Planetary Camera 2 on board the Hubble Space Telescope, described in Sarajedini et al. (2000). The clusters are in all cases roughly centered on the Planetary Camera (PC) chip. Each dataset contained expo-

tures in the F555W (V) and F814W (I) bands, allowing for two independent sets of measurements for each cluster.

From visual inspection of the WFPC2 images (Figs 1, 2, 4 and 6 in Sarajedini et al. 2000) it is clear that none of the clusters are strongly elongated. We used the ELLIPSE task in the STSDAS package in IRAF to fit elliptical isophotes to the cluster images, after filtering the images with an 11×11 pixels median filter to create the smooth profiles required by ELLIPSE. Fig. 3 shows the position angle (N through E) and ellipticity as a function of semi-major axis for each cluster and confirms that all clusters have small ellipticities. For radii less than about $0''.5$, the smoothing and random fluctuations due to individual stars make the fits meaningless. For H38 and M9, strong variations in the position angle are seen also at larger radii, most likely because the ellipticities are so small that the PA is very poorly constrained. U49 is the only one of the four clusters where visual inspection of the images hints at some elongation, and the ELLIPSE fits yield an ellipticity of $\epsilon \approx 0.10$ – 0.15 for this cluster, with a relatively stable PA around 30 degrees. For the remaining clusters the ellipticities are less than ~ 0.1 , consistent with the mean value of 0.07 ± 0.01 for Milky Way globulars (White & Shawl 1987) and also in good agreement with the mean $\epsilon = 0.11 \pm 0.01$ for M31 GCs (Barmby, Holland, & Huchra 2002).

Additional structural parameters for the clusters were derived by fitting single-mass King–Michie models (King 1966, hereafter simply “King” models) to the WFPC2 images. Because the ellipticities are generally small and the position angles ill-determined and possibly varying with radius, we simply assumed circularly symmetric profiles for the model fits. We then carried out a least-squares fit directly to the images, solving for the core radius r_c , concentration parameter W and central surface brightness μ_0 . The minimization was done with the downhill simplex (“amoeba”) algorithm described in *Numerical Recipes* (Press et al. 1992). Although the clusters are quite well resolved, crowding near the center and strongly variable completeness functions as a function of radial distance made direct starcounts unfeasible. For the same reasons, attempts to subtract individual stars from the images might also lead to systematic errors in the derived profiles. Assuming that field stars are uniformly distributed throughout the frames, we decided that the approach that would be least likely to suffer from systematic effects due to partial resolution of the clusters was to simply fit the King models to the images directly. The background level was determined as the average of all pixel values in an annulus centered on the cluster, with an inner radius of 200 pixels (9 arcsec) and 100 pixels wide. This is about the largest possible background annulus that could be consistently used, considering variations in the exact position of the clusters on the PC chip and the limited field size. The fit itself was carried out for radii less than 200 pixels. We also attempted to solve for the centroid of the profile simultaneously, but these fits turned out to be unstable and we found that a more reliable approach was to determine the center of the profiles by carrying out the fits for various central positions and inspecting the residuals. Even for fairly small centering errors ($\lesssim 1$ pixel), asymmetries in the residuals were clearly visible.

As noted by other authors (Chandar, Bianchi, & Ford 2001; Barmby, Holland, & Huchra 2002), the effect of the HST PSF is not entirely negligible when measuring structural parameters for star

clusters in M31 or M33. Our modeling included a convolution of the 2-d King profiles with the PC PSF, generated by the TINYTIM software³ and, like previous studies, we found small but measurable differences in the fits when the PSF convolution was included. Core and effective radii were typically ~ 0.1 pc ($\sim 0''.02$) smaller, while the central surface brightnesses μ_0 increased by 0.1–0.2 mag with PSF convolution.

Fits to the F555W images are shown in Fig. 4. The error bars indicate the actual cluster profiles while the solid lines are the King model fits. The light profiles were measured in concentric apertures with the PHOT task within DAOPHOT in IRAF, measuring the sky background in the same annuli that were used for the fits. Note that, because of the 2-d fitting procedure, the solid lines are *not* direct fits to the actual datapoints in Fig. 4, but are measured on the best-fitting convolution product of a 2-d King profile and the PC PSF, using the same procedure as for the cluster profiles. The King models generally provide excellent fits to the globular cluster profiles. In particular, we see no evidence for central cusps that might indicate core-collapsed clusters. The fitted parameters are listed in Table 2, with separate fits for the F555W and F814W images. Uncertainties were estimated by repeating the fitting procedure 18 times using different initial values for r_c , W and μ_0 . We have adopted the standard deviation on each fitted parameter, rather than the standard error on the mean, as our uncertainty estimates. Alternatively, the difference between the F555W and F814W fits may be used as an estimate of the uncertainties, and provides similar uncertainty estimates to those in Table 2.

Cluster R12 was also measured by Chandar, Bianchi, & Ford (1999). Although they fitted the empirical version (King 1962) of the King models rather than the theoretical King–Michie models used here, the two types of King models are structurally similar enough that a comparison of the derived core radii is illustrative. Fitting a King (1962) profile to the F555W image, Chandar et al. found a core radius of $0''.234$ for R12 which is only slightly larger than our value of $0''.225$ (corrected for the PSF). Without correction for the PSF we get $r_c = 0''.253$, now slightly larger than the Chandar et al. value. The small differences between our measurements and those of Chandar et al. can easily be ascribed to the different choices of King profiles and fitting procedure, small centering errors etc.

In addition to the three basic parameters r_c , W and μ_0 , Table 2 also includes the parameter C , which is the ratio of the tidal radius r_t to the core radius r_c , as well as the effective radius r_e , defined as the radius containing half the cluster light in projection. These two additional parameters both follow directly from the King model r_c and W parameters, but are listed for convenience.

One potential concern is that the tidal radius for one of the clusters, U49, is larger than the inner radius of the sky annulus, leading to possible systematic errors in the sky background determination. For the best-fitting model, a sky background level of about 0.2 ADU is expected at $r = 200$ pixels, decreasing rapidly outwards. We tried varying the background level by ± 0.5

³Available at the URL <http://www.stsci.edu/software/tinytim/tinytim.html>

ADU and redid the fits for U49. The core and effective radii were affected by less than $0''.05$ (0.2 pc) while the dimensionless C parameter changed by about 1, i.e. the changes were in both cases comparable to the uncertainties in Table 2.

The core and effective radii for the M33 clusters are well within the range spanned by Milky Way globular clusters. The r_c distribution for Milky Way GCs peaks at about 1 pc, but has a tail extending up to above 10 pc. Excluding core-collapsed clusters, the median value is 1.3 pc. The median half-light radius r_e for Milky Way GCs is 3.3 pc (using values from Harris 1996), but the distribution is again strongly asymmetric. It may be worth noting that the reddest M33 cluster (R12, see sect 2.3) also has the smallest effective radius, an effect that has been observed in many other galaxies including the Milky Way and M31 (e.g. Barmby, Holland, & Huchra 2002; Larsen et al. 2001). Another point of interest is that previous studies of Milky Way and M31 globular clusters have found that low-concentration clusters tend to be more elliptical (Barmby, Holland, & Huchra 2002), which is consistent with U49 being the most elongated as well as the largest of the clusters in our sample. However, the 4 clusters studied here clearly constitute a too small sample to draw conclusions as to whether or not the same effects are generally present in M33.

2.3. Integrated photometry

Fig. 5 shows the integrated V magnitudes of the clusters as a function of radius. The curves-of-growth are drawn with dashed lines beyond the tidal radii obtained from the King profile fits. The background level was determined in the same way as for the King profile fits and the number counts in F555W and F814W in each aperture were converted to V magnitudes and $V-I$ colors using the transformations in Holtzman et al. (1995). Because the Holtzman et al. zero-points include an implicit -0.1 mag aperture correction from their $r = 0''.5$ reference aperture to infinity, which does not apply in our case, we have added 0.1 mag to the magnitudes. Apart from small color terms, this gives exactly the same results as using the photometric zero-points in the image headers directly.

The curve-of-growth for M9 has a “bump” at $r = 200$ pixels, due to a bright star that is located just within the outer aperture radius, but the curves are otherwise smooth and monotonically increasing over most of the radial range. For a couple of clusters (R12 and H38), the curves decrease slightly at large radii, reflecting the inherent uncertainties in the background determination. A small decrease of 0.5–1.0 ADU in the background levels would make the curves-of-growth for R12 and H38 increase monotonically out to their tidal radii.

Both Christian & Schommer (1988, hereafter CS88) and Chandar, Bianchi, & Ford (2001, CBF01) have published integrated photometry for the 4 clusters, using ground-based CCD imaging and WFPC2 data, respectively. In Table 3 we compare our photometry with CS88 and CBF01. CS88 used an aperture radius of $3''.7$, corresponding to 82 pixels on the PC camera, while CBF01 used an aperture of $2''.2$ (48 pixels) for H38, M9 and R12 and $2''.7$ (59 pixels) for U49. We redid the photometry in the same apertures used by CBF01 and CS88 as well as in a larger aperture.

For R12 and H38 this larger aperture coincided with the tidal radii of the clusters, for M9 we used an aperture of $r = 190$ pixels (to avoid the bright star) and for U49 we used $r = 200$ pixels. For the comparison with CBF01 we used the same background annulus as they did ($3''.5 < r < 5''$), but for the other measurements the same annulus was used as for the King model fits and the curves-of-growth.

While our $V-I$ color measurements agree fairly well with those of CBF01, our V magnitudes are systematically fainter than theirs by about 0.18 mag. Part of this discrepancy is due to the fact that no correction was applied to the Holtzman et al. zeropoints in CBF01 (Chandar, priv. comm.). By experimenting with the PHOT options, we found that the remaining 0.08 mag can be accounted for by differences in the background level estimates. Because the resolution into individual stars makes the sky histogram highly asymmetric, the background measurements in these fields are very sensitive to the choice of algorithm. Specifically, if we use the MODE option (as did CBF01) instead of simply calculating the mean, the discrepancy is reduced to a few times 0.01 mag. However, because the contribution from individual, resolved stars is part of the “sky” background within the photometric apertures and therefore needs to be subtracted, a simple mean appears to be the most appropriate background estimator for our purpose.

Our photometry in the $3''.7$ aperture agrees closely with that of CS88, being only 0.02 mag fainter on the average. For some clusters the curves-of-growth continue to rise well beyond $3''.7$, and the measurements in Table 3 suggest that this aperture may underestimate the luminosity of the most extended cluster, U49, by ~ 0.2 mag. However, measurements in the largest apertures are quite sensitive to uncertainties in the background level, and for R12 and H38 the integrated magnitudes in the largest aperture are actually slightly fainter than in the $3''.7$ aperture, in accordance with the behavior of the curves-of-growth pointed out above. The small adjustments in the background level that would make the curves-of-growth monotonic would affect the photometry at $r = 50$ pixels ($2''.3$) by only ~ 0.02 mag, but at the tidal radii the changes amount to 0.1–0.2 mag. This may provide a more realistic estimate of the true uncertainty on the integrated photometry than pure photon statistics, which give formal errors of less than 0.002 mag. In practice, the uncertainty on the background level is dominated by stochastic variations in the numbers of individual, bright stars within the aperture annulus, as well as true variations due to dust obscuration etc. A larger field of view would help reduce the stochastic variations, but would increase the sensitivity to large-scale variations in the background. For the following discussion we will use our photometry in columns (10) and (11) of Table 3 as the best approximation to the total integrated magnitudes of the clusters.

3. Masses and mass-to-light ratios

Once the velocity dispersion and structural parameters of a cluster are known, the total mass can be estimated. The simplest way is to use the virial theorem which implies

$$M_{\text{vir}} = a \frac{\sigma_{3D}^2 r_h}{G} \quad (1)$$

where the constant a has a value of 2.5 (Spitzer 1987, p. 11). In this expression, σ_{3D} is the three-dimensional velocity dispersion, $\sigma_{3D}^2 = 3\sigma_x^2$, and r_h is the 3-dimensional half-*mass* radius which is generally larger than the projected half-*light* radius r_e by a factor of 4/3. In the present case, however, the King model fits allowed r_h to be directly evaluated for each individual cluster, without using r_e as an intermediate step. An alternative method is to use “Kings formula” (Richstone & Tremaine 1986; Queloz, Dubath, & Pasquini 1995),

$$M_{\text{king}} = \frac{9}{2\pi G} \frac{\mu r_c \sigma_0^2}{\alpha p} \quad (2)$$

Here σ_0 is the *central* (projected) velocity dispersion and r_c is the core radius of the cluster. The remaining parameters, μ (a dimensionless mass, not to be confused with the central surface brightness μ_0), p (ratio of central surface density to central 3-d density) and α (ratio of half-width at half maximum to core radius, usually close to 1) are all functions of the concentration parameter and were again evaluated using the King model fits.

The velocity dispersion σ_{3D} used in (1) is the mean value averaged over the entire cluster, while the σ_0 used in (2) is the central value. Neither of these is the actual observed value σ_x , since a slit of finite size was used for the observations. Using the King model fits, which provide the velocity dispersion in the cluster as a function of radius, we estimated the aperture corrections from our slit to the central and global values, assuming a slit width of $0.72''$ (3.2 pc at the distance of M33) and infinite length. The aperture corrections are relatively modest, generally amounting to less than 10% in either direction.

It should be noted that both methods implicitly assume a constant M/L ratio as a function of radius and isotropic velocity distributions. In practice, some mass segregation is expected because of equipartition of energy, and has indeed been detected observationally in some cases (e.g. King, Sosin, & Cool 1995; Ferraro et al. 1997; Sosin 1997). The King models used here are single-mass models and certainly an oversimplification of the true dynamical situation in the clusters, but in practice the difference between dynamical masses obtained by fitting single-mass King models and more sophisticated methods tends to be relatively small (e.g. Djorgovski 1995; Meylan et al. 2001). Anisotropy is expected to occur mostly in the outer parts of the clusters (Gunn & Griffin 1979; Lupton, Gunn, & Griffin 1987; Takahashi & Lee 2000) and should not have a strong impact on M/L ratios derived from the integrated light.

The computed central and global (σ_∞) velocity dispersions are listed in Table 4, col. (2) and (3). Columns (4) and (5) give the corresponding King and virial masses, using the structural parameters

measured on the F555W frames. Considering that neither the rms nor the standard errors on the mean are likely to provide realistic estimates of the true errors on the velocity dispersions, we have adopted 0.5 km/s for the errors on σ_x , corresponding roughly to the typical difference between the measurements based on direct fit and cross-correlation. We have omitted errors on σ_∞ and σ_0 in Table 4 since these scale, at least to first order, with the errors on σ_x . Column (6) lists the central density in $M_\odot \text{pc}^{-3}$ which, per definition, is $\rho_0 = M_{\text{King}}/(\mu r_c^3)$. The V -band (King) mass-to-light ratios, M/L_V , are given in col. (7) and column (8) lists the binding energy of each cluster, calculated as in McLaughlin (2000). For the mass-to-light ratios we have used the V magnitudes in Table 3 and the distance modulus of 24.84 and the reddenings of individual clusters given in Sarajedini et al. (2000). Other estimates of the distance modulus of M33 are $24.52 \pm 0.14(\text{random}) \pm 0.13(\text{systematic})$ (Lee et al. 2002, based on Cepheids), $24.81 \pm 0.04(\text{random}) \pm 0.05(\text{systematic})$ (Kim et al. 2002, red giants), and 24.64 ± 0.09 (Freedman, Wilson, & Madore 1991, Cepheids). The derived M/L ratios are inversely proportional to the assumed distance, and could be underestimated by up to 14% if the smallest of the above distances is correct.

As seen from Table 4, the virial and King masses are generally very similar. This agreement is not entirely fortuitous, since the two estimates are not independent. In fact, the ratio $M_{\text{King}}/M_{\text{vir}}$ is

$$\frac{M_{\text{King}}}{M_{\text{vir}}} \propto \frac{\mu}{\alpha p} \frac{r_c}{r_h} \frac{\sigma_0^2}{\sigma_{3D}^2} \quad (3)$$

where the constants have been excluded. Since all the factors in Eq. 3 are functions of the concentration parameter only, this is also true for $M_{\text{King}}/M_{\text{vir}}$. This ratio is plotted in Fig. 6 and is evidently very close to 1 for the relevant range of concentration parameters.

The average of the M/L_V ratios in Table 4, $\langle M/L_V \rangle = 1.53 \pm 0.18$, is in excellent agreement with McLaughlin’s 1.45 ± 0.1 value for the core M/L_V of Milky Way GCs. Cluster R12 formally has a somewhat lower M/L_V than the other three clusters, but we note that this is also the most compact of the clusters and it is possible that the effects of mass segregation and departures from the single-mass King model approximation are more pronounced here. For 6 clusters in M31 with HST imaging, Dubath & Grillmair (1997) obtain a mean M/L_V ratio of $\langle M/L_V \rangle = 1.2 \pm 0.21$ or $\langle M/L_V \rangle = 2.0 \pm 0.44$, based on King model fits and use of the virial theorem, respectively. These estimates nicely bracket our mean value for the M33 clusters. If we had used the velocity dispersions based on the direct fitting instead of those obtained by cross-correlation, the masses (and resulting M/L_V ratios) would have increased by $\sim 20\%$, still in good agreement with the Milky Way value.

4. Fundamental plane relations

We finally explore how the M33 clusters fit into the “fundamental plane” relations obeyed by Milky Way globular clusters. Figure 7 shows our M33 data compared with data for Milky Way GCs, taken from Pryor & Meylan (1993) and Harris (1996). Core-collapsed Milky Way clusters

have been omitted from the plots. Panels (a) and (b) show the bivariate core parameter relations (Djorgovski 1995), with Milky Way GCs plotted as + symbols and M33 clusters as filled circles. As shown by Djorgovski, both of these relations are consistent with GCs being virialized systems with a constant M/L ratio. The M33 clusters fit remarkably well onto the the fundamental plane relations obeyed by the Milky Way clusters, consistent with their similar mass-to-light ratios. We note that Barmby, Holland, & Huchra (2002) found slight deviations between the fundamental plane relations for their sample of M31 globular clusters and the Milky Way data, but it is unclear to what extent those differences are due to systematic measurement errors or real physical differences between the GCs in the two galaxies.

Panel (c) shows the cluster binding energies as a function of absolute V magnitude, M_V . McLaughlin (2000) found a tight relation between these two quantities for Milky Way GCs, with an additional weaker dependence on Galactocentric distance r_{gc} . He gave the relation as

$$\log(E_b/\text{ergs}) = [(39.86 \pm 0.40) - 0.4 \log(r_{gc}/8\text{kpc})] + (2.05 \pm 0.08) \log(L/L_\odot).$$

For the four M33 globular clusters we find a mean value of $\langle \log(E_b L^{-2.05}) \rangle = 39.81$, with a scatter of only 0.13 dex. Ignoring the term in r_{gc} , we thus find once again that the M33 globular clusters fall nearly exactly on the same relation as the Milky Way globular clusters.

The similarity to Milky Way GCs in general, and in the mass-to-light ratios in particular for M33 clusters is interesting in the context of the results by Sarajedini et al. (1998) and Chandar et al. (2002), since a younger age should generally imply lower M/L ratios unless there is an excess of low-mass stars. For a Miller-Scalo IMF, for example, population synthesis models by Bruzual & Charlot (priv. comm.) predict an increase in M/L_V of about a factor of 2 from 5 Gyrs to 12 Gyrs, and a factor ~ 5 from 2 Gyrs to 12 Gyrs. Indeed, Fischer, Welch, & Mateo (1992) find a much lower M/L ratio ($M/L_V \lesssim 0.2$) for the ~ 2 Gyr old cluster NGC 1978 in the LMC than for any of the clusters studied here. However, a younger age for the M33 clusters is still possible if a steeper IMF slope conspires with a young age to produce the same M/L. Of our four GCs, Chandar et al. (2002) list spectroscopic age estimates for U49 (12–17 Gyrs) and H38 (5 Gyrs), but we note that absolute ages based on integrated spectra are still uncertain (e.g. Schiavon et al. 2002). On the other hand, if H38 and U49 are both old clusters ($\gtrsim 10$ Gyr), then alternative explanations will be required for their excessively red horizontal branch morphologies, the presence of stars above their RGB tips, and their anomalously bright red clump magnitudes (Sarajedini et al. 1998, 2000). Clearly, more work needs to be done before the question of a real, large age spread among M33 halo GCs can be answered with confidence.

5. Summary

We have measured velocity dispersions for 4 old “halo” globular clusters in M33 and combined these with structural parameters from WFPC2 images to obtain mass-to-light ratios for the clusters. Our analysis shows that the M33 GCs have M/L_V ratios essentially identical to those of GCs in

the Milky Way and M31, as well as similar structural parameters (core- and effective radii). The M33 clusters also fall on the same “fundamental plane” and binding energy vs. luminosity relations as Milky Way and M31 clusters (Djorgovski 1995; Dubath & Grillmair 1997; McLaughlin 2000). Unless the stellar IMFs in these clusters have an excess of low-mass stars relative to GCs in the Milky Way, the similarity in M/L ratios and the fundamental plane relations suggest similar high ages. It would be very interesting to measure velocity dispersions for M33 clusters spanning a wide range of ages and look for the expected variations in M/L ratio.

This work was supported by National Science Foundation grant number AST9900732 and by NSF Career Grant No. AST0094048. JPH was supported by the Smithsonian Institution. This research has made use of the SIMBAD database, operated at CDS, Strasbourg, France. We thank Rupali Chandar for helping to sort out the differences between our photometry and hers, and the Keck staff for their assistance with the observations.

REFERENCES

- Barmby, P. & Huchra, J. P., 2000, *ApJ*, 531, 29
- Barmby P., Huchra J. P., Brodie J. P., et al., 2000, *AJ*, 119, 727
- Barmby, P., Holland, S., & Huchra, J. P. 2002, *AJ*, 123, 1937
- Buonanno, R., Corsi, C. E., Pulone, L., Fusi Pecci, F., & Bellazzini, M. 1998, *A&A*, 333, 505
- Chandar, R., Bianchi, L., & Ford, H. C. 1999, *ApJ*, 517, 668
- Chandar, R., Bianchi, L., & Ford, H. C. 2001, *A&A*, 366, 498
- Chandar, R., Bianchi, L., Ford, H. C., & Sarajedini, A. 2002, *ApJ*, 564, 712
- Christian, C. A. & Schommer, R. A. 1982, *ApJS*, 49, 405
- Christian, C. A. & Schommer, R. A. 1988, *AJ*, 95, 704
- Djorgovski, S. 1995, *ApJ*, 438, L29
- Djorgovski, S. G., Gal, R. R., McCarthy, J. K., Cohen, J. G., de Carvalho, R. R., Meylan, G., Bendinelli, O., & Parmeggiani, G. 1997, *ApJ*, 474, L19
- Dubath, P. & Grillmair, C. J. 1997, *A&A*, 321, 379
- Elmegreen B.G., Efremov Y.N. 1997, *ApJ*, 480, 235
- Ferraro, F. R., Carretta, E., Bragaglia, A., Renzini, A., & Ortolani, S. 1997, *MNRAS*, 286, 1012
- Fischer, P., Welch, D. L., & Mateo, M. 1992, *AJ*, 104, 1086
- Freedman, W. L., Wilson, C. D., & Madore, B. F. 1991, *ApJ*, 372, 455
- Girardi, L., Chiosi, C., Bertelli, G., Bressan, A. 1995, *A&A*, 298, 87
- Gunn, J. E. & Griffin, R. F. 1979, *AJ*, 84, 752
- Harris, W. E. 1996, *AJ*, 112, 1487
- Hiltner, W. A. 1960, *ApJ*, 131, 163
- Ho, L. C., Filippenko, A. V., 1996b, *ApJ*, 472, 600
- Hodge, P. W. 1961, *ApJ*, 133, 413
- Holtzman, J. A., Burrows, C. J., Casertano, S., et al. 1995, *PASP*, 107, 1065
- Illingworth, G., 1976, *ApJ*, 204, 73

- Jablonka, P., Bica, E., Bonnatto, C., et al., 1998, *A&A*, 335, 867
- Kim, M., Kim, E., Lee, M. G., Sarajedini, A., & Geisler, D. 2002, *AJ*, 123, 244
- Kinman T. D., 1959, *MNRAS*, 119, 538
- King, I. R. 1962, *AJ*, 67, 471
- King, I. R. 1966, *AJ*, 71, 64
- King, I. R., Sosin, C., & Cool, A. M. 1995, *ApJ*, 452, L33
- Kormendy, J. 1985, *ApJ*, 295, 73
- Kron, G. E. & Mayall, N. U. 1960, *AJ*, 65, 581
- Larsen, S. S., Brodie, J. P., Huchra, J. P., Forbes, D. A., & Grillmair, C. J. 2001, *AJ*, 121, 2974
- Lee, M. G., Kim, M., Sarajedini, A., Geisler, D., & Gieren, W. 2002, *ApJ*, 565, 959
- Lupton, R. H., Gunn, J. E., & Griffin, R. F. 1987, *AJ*, 93, 1114
- McLaughlin, D. E. 2000, *ApJ*, 539, 618.
- Meylan, G., Sarajedini, A., Jablonka, P., Djorgovski, S. G., Bridges, T., & Rich, R. M. 2001, *AJ*, 122, 830
- Minniti, D., 1995, *AJ*, 109, 1663
- Murray S.D., Lin D.N.C. 1992, *ApJ*, 400, 265
- Perrett, K. M., Bridges, T. J., Hanes, D. A., Irwin, M. J., Brodie, J. P., Carter, D., Huchra, J. P., & Watson, F. G. 2002, *AJ*, 123, 2490
- Press, W. H., Teukolsky, S. A., Vetterling, W. T., Flannery, B. P., 1992 *Numerical Recipes in C/Fortran*, Cambridge University Press
- Pryor, C. & Meylan, G. 1993, *ASP Conf. Ser. 50: Structure and Dynamics of Globular Clusters*, 357
- Queloz, D., Dubath, P., & Pasquini, L. 1995, *A&A*, 300, 31.
- Richstone, D. O. & Tremaine, S. 1986, *AJ*, 92, 72.
- Rosenberg, A., Saviane, I., Piotto, G., & Aparicio, A. 1999, *AJ*, 118, 2306
- Sarajedini, A., Chaboyer, B., & Demarque, P. 1997, *PASP*, 109, 1321
- Sarajedini, A., Geisler, D., Harding, P., & Schommer, R. 1998, *ApJ*, 508, L37

- Sarajedini, A., Geisler, D., Schommer, R., & Harding, P. 2000, *AJ*, 120, 2437
- Schiavon, R. P., Faber, S. M., Rose, J. A., Castilho, B. V., 2002, *AJ*, submitted (astro-ph/0109365)
- Schommer, R. A., Christian, C. A., Caldwell, N., Bothun, G. D., & Huchra, J. 1991, *AJ*, 101, 873
- Sosin, C. 1997, *AJ*, 114, 1517
- Spitzer, L. 1987, “Dynamical Evolution of Globular Clusters”, Princeton Series in Astrophysics, Princeton University Press
- Stetson, P. B., Vandenberg, D. A., & Bolte, M. 1996, *PASP*, 108, 560
- Takahashi, K. & Lee, H. M. 2000, *MNRAS*, 316, 671
- Tonry, J. & Davis, M. 1979, *AJ*, 84, 1511
- Vogt, S. S. et al. 1994, *Proc. SPIE*, 2198, 362
- White, R. E. & Shawl, S. J. 1987, *ApJ*, 317, 246
- Zinn, R., 1985, *ApJ*, 293, 424

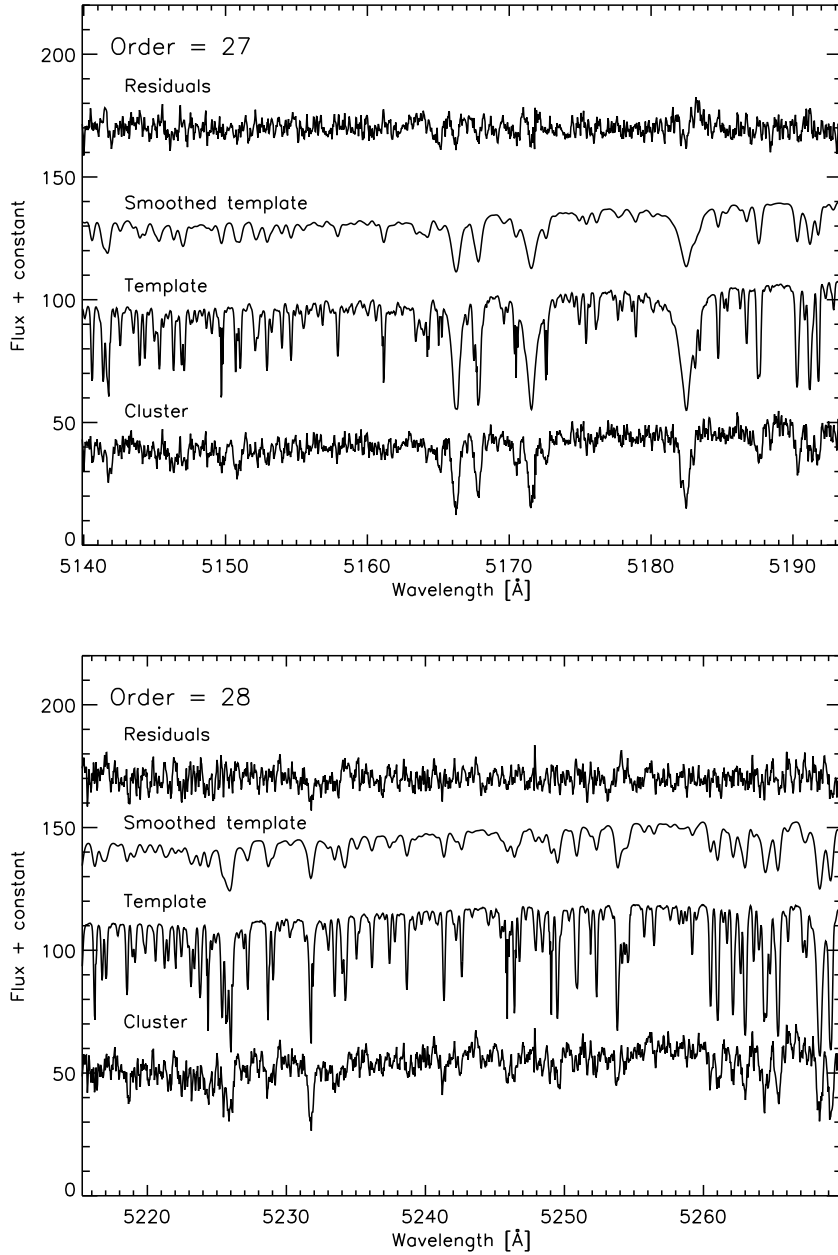


Fig. 1.— Comparison of cluster spectra and template star spectra for two echelle orders of the cluster M33-H38. All spectra are normalized in the same way, but zero-point offsets have been applied for clarity. Order 27 includes the region around the Mgb triplet.

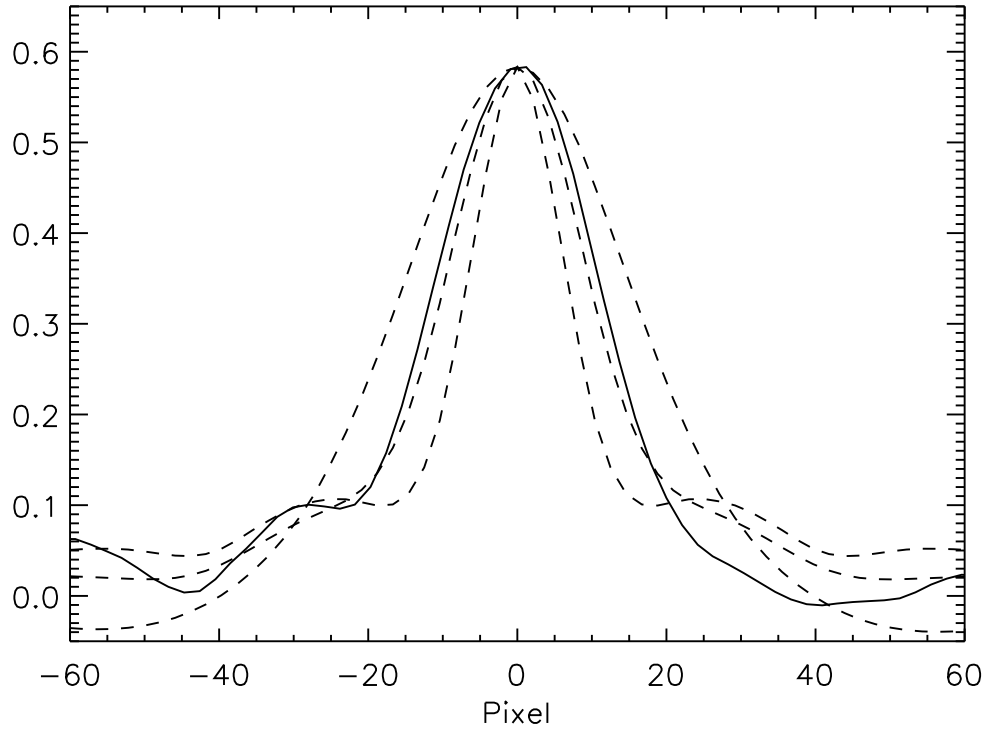


Fig. 2.— Cross-correlation for template star vs. cluster H38 (solid line) and template star broadened with Gaussian profiles corresponding to $\sigma_x = 0, 6 \text{ km/s}$ and 12 km/s (dashed lines).

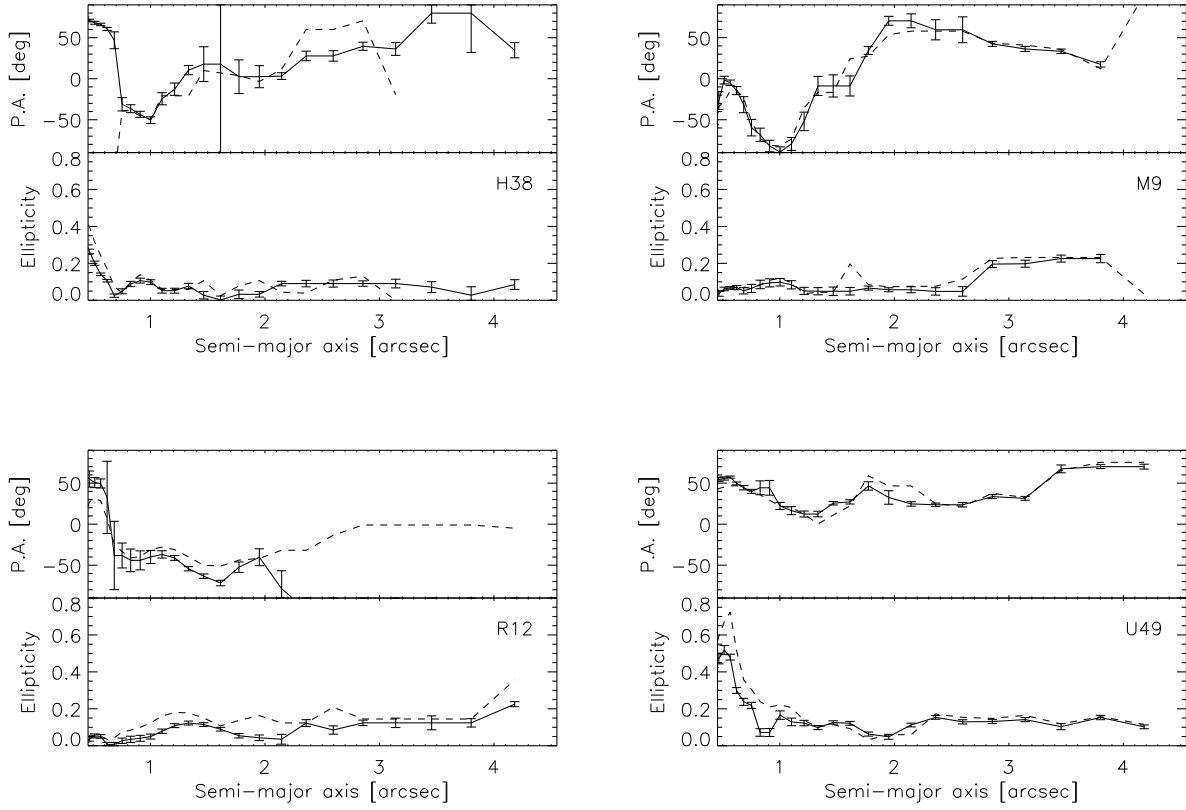


Fig. 3.— Ellipticities and major axis position angles for the four globular clusters. Solid and dashed lines indicate fits to F555W and F814W images, respectively. Position angles are counted N through E.

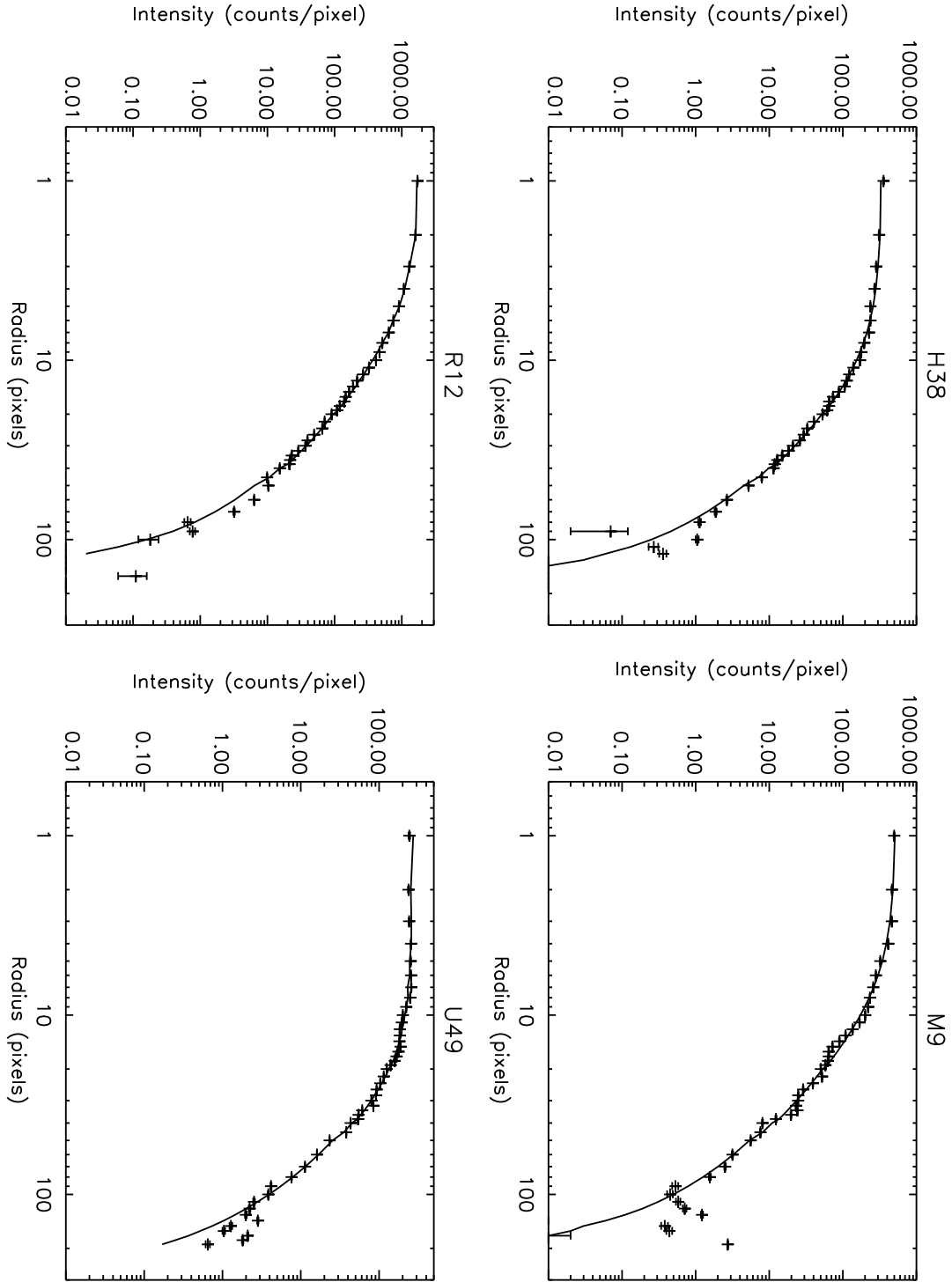


Fig. 4.— Surface brightness profiles and King profile fits for HST images of the 4 globular clusters in M33.

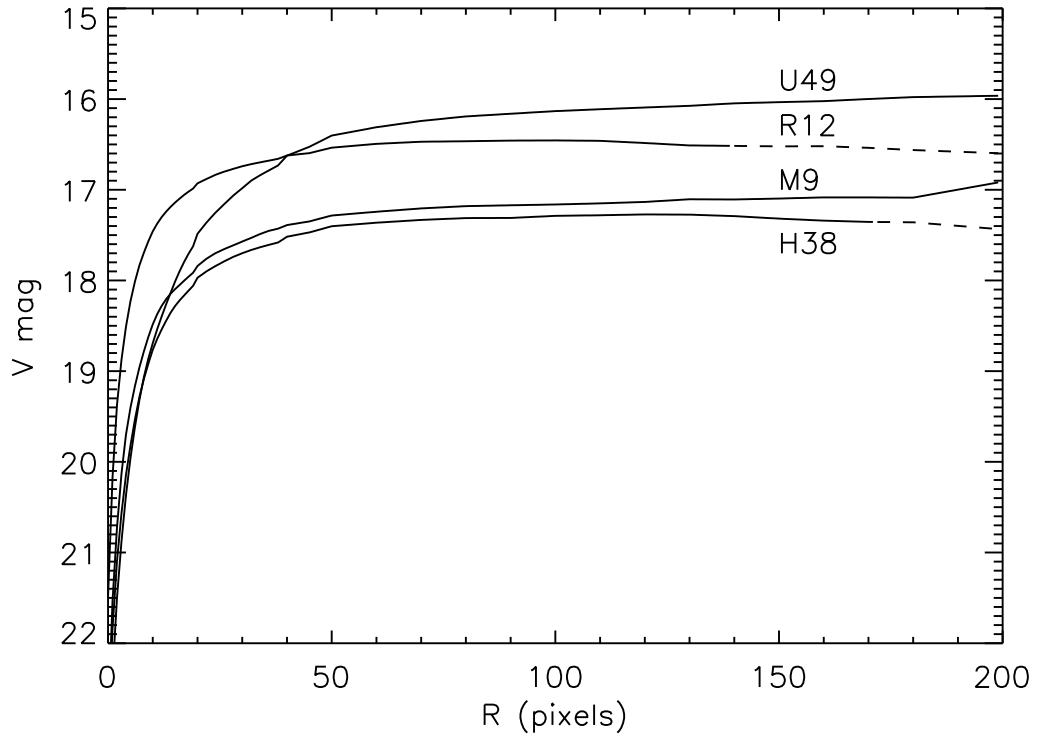


Fig. 5.— Curves-of-growth for the globular clusters. The curves are drawn with dashed lines beyond the tidal radii inferred from the King model fits.

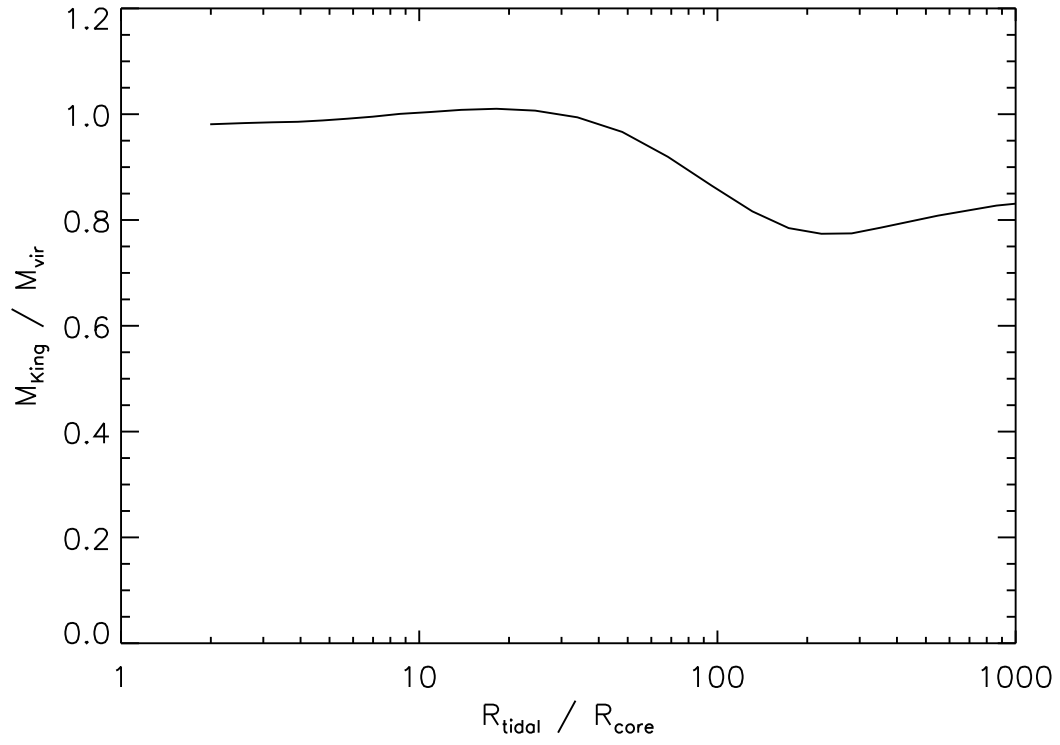


Fig. 6.— Ratio of King mass to virial mass as a function of concentration parameter.

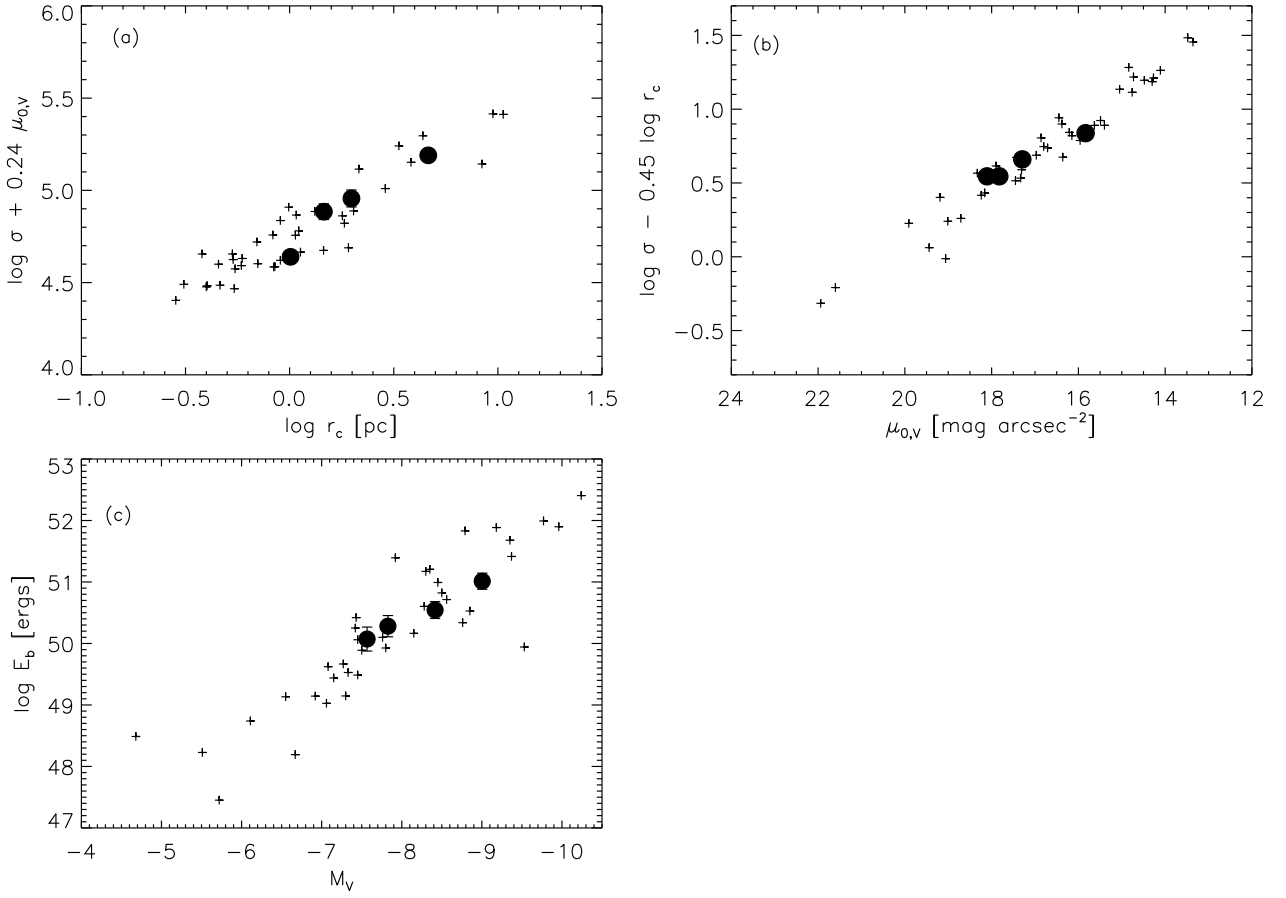


Fig. 7.— Fundamental plane correlations for Milky Way (+ symbols) and M33 globular clusters (filled circles).

Table 1. Radial velocities and measured velocity dispersions.

ID	N	v_r km/s	v_r (S91) km/s	v_r (C02) km/s	σ_x	rms	err	σ_x	rms	err
(1)	(2)	(3)	(4)	(5)	(6)	Direct fit		Cross-correlation		
						(7)	(8)	(9)	(10)	(11)
H38	26	-195.4 ± 0.8	-100 ± 100	-254 ± 20	5.33	1.29	0.25	4.42	0.84	0.16
M9	21	-202.4 ± 1.1	-300 ± 40	-213 ± 10	5.57	0.98	0.21	5.01	1.02	0.22
R12	19	-218.4 ± 0.7	-190 ± 40	-218 ± 10	6.69	0.37	0.08	6.31	0.52	0.12
U49	19	-149.8 ± 1.5	-180 ± 40	-157 ± 16	7.04	0.90	0.21	6.52	1.18	0.27

Note. — N is the number of echelle orders used. The measured line-of-sight velocity dispersions, σ_x , are in km/s. For comparison we have included radial velocities from Schommer et al. (1991) and Chandar et al. (2002).

Table 2. King model parameters.

ID	r_c pc	W	μ_0 mag arcsec $^{-2}$	C	r_e pc
(1)	(2)	(3)	(4)	(5)	(6)
F555W					
H38	1.98 ± 0.07	5.97 ± 0.22	17.90 ± 0.03	17.8 ± 2.1	3.94 ± 0.16
M9	1.46 ± 0.10	6.74 ± 0.38	17.37 ± 0.06	28.3 ± 6.3	3.88 ± 0.38
R12	1.01 ± 0.02	6.76 ± 0.12	15.93 ± 0.02	28.4 ± 2.2	2.67 ± 0.10
U49	4.63 ± 0.20	5.40 ± 0.28	18.24 ± 0.03	13.1 ± 1.9	7.81 ± 0.33
F814W					
H38	2.09 ± 0.13	5.44 ± 0.40	16.78 ± 0.05	13.6 ± 2.4	3.57 ± 0.18
M9	1.54 ± 0.07	6.70 ± 0.26	16.42 ± 0.04	27.7 ± 4.8	3.99 ± 0.34
R12	1.11 ± 0.03	6.43 ± 0.13	14.85 ± 0.03	23.1 ± 1.8	2.59 ± 0.07
U49	4.48 ± 0.18	5.53 ± 0.26	17.18 ± 0.03	14.0 ± 1.8	7.83 ± 0.28

Note. — Concentration parameter C and effective radius r_e are derived from r_c and W . Central surface brightnesses have not been corrected for reddening.

Table 3. Integrated photometry for the clusters. No corrections for reddening have been applied.

ID	CS88		CBF01		This work					
	V	$V-I$	V	$V-I$	r as in CBF01		r as in CS88		$r = \text{tidal}$	
					V	$V-I$	V	$V-I$	V	$V-I$
(1)	(2)	(3)	(4)	(5)	(6)	(7)	(8)	(9)	(10)	(11)
H38	17.26	...	17.25	1.07	17.43	1.11	17.31	1.07	17.35	1.09
M9	17.17	1.06	17.16	1.02	17.33	1.05	17.18	1.06	17.09	1.06
R12	16.38	1.19	16.37	1.15	16.55	1.17	16.46	1.17	16.52	1.19
U49	16.24	1.17	16.23	1.03	16.43	1.03	16.19	1.03	15.97	1.00

Table 4. Mass estimates, central densities and mass-to-light ratios.

ID	σ_0	σ_∞	M_{king}	M_{vir}	ρ_0	$(M/L)_V$	E_b
	km/s	km/s	$\times 10^5 M_\odot$		$M_\odot \text{pc}^{-3}$		$\times 10^{50}$ ergs
(1)	(2)	(3)	(4)	(5)	(6)	(7)	(8)
H38	4.77	3.99	1.46 ± 0.33	1.44 ± 0.33	1200 ± 300	1.65 ± 0.37	1.18 ± 0.53
M9	5.42	4.46	1.77 ± 0.35	1.77 ± 0.35	2500 ± 700	1.57 ± 0.31	1.91 ± 0.76
R12	6.91	5.69	2.00 ± 0.32	2.00 ± 0.32	8600 ± 1500	1.03 ± 0.16	3.50 ± 1.11
U49	6.99	5.88	6.23 ± 0.96	6.20 ± 0.95	460 ± 90	1.87 ± 0.29	10.3 ± 3.1

Note. — σ_0 and σ_∞ are the central and global 1-d velocity dispersions, derived from the observed velocity dispersions σ_x in Table 1 based on the cross-correlation technique.